

Epidemiological short-term Forecasting with Model Reduction of Parametric Compartmental Models. Application to the first pandemic wave of COVID-19 in France.

Athmane Bakhta, Thomas Boiveau, Yvon Maday, Olga Mula

Abstract

We propose a forecasting method for predicting epidemiological health series on a two-week horizon at the regional and interregional level. The approach is based on model order reduction of parametric compartmental models, and is designed to accommodate small amount of sanitary data. The efficiency of the method is examined in the case of the prediction of the number of hospitalized infected and removed people during the first pandemic wave of COVID-19 in France, which has taken place approximately between February and May 2020. Numerical results illustrate the promising potential of the approach.

1 Introduction

Providing reliable epidemiological forecasts during an ongoing pandemic is crucial to mitigate the potentially disastrous consequences on global public health and economy. As the ongoing pandemic on Covid-19 sadly illustrates, this is a daunting task in the case of new diseases due to the incomplete knowledge of the behavior of the disease, and the heterogeneities and uncertainties in the health data count. Despite these difficulties, many forecasting strategies exist and we could cast them into two main categories. The first one is purely data-based, and involves statistical and learning methods such as time series analysis. The second approach uses epidemiological models which are appealing since they provide an interpretable insight of the mechanisms of the outbreak. They also provide high flexibility in the level of detail to describe the evolution of the pandemic, ranging from simple compartmental models that divide the population into a few exclusive categories, to highly detailed descriptions involving numerous compartments or even agent-based models (see, e.g., [5, 2]). The salient drawback of using epidemiological models for forecasting purposes lies in the very high uncertainty in the estimation of the involved parameters. This is due to the fact that most of the time the parameters cannot be inferred from real observations and the available data are insufficient or too noisy to provide any reliable estimation. The situation is aggravated by the fact that the number of parameters can quickly become large even in moderately simple compartmental models. As a result, forecasting with these models involves making numerous a priori hypothesis which can sometimes be hardly justified by data observations.

In this paper, our goal is to forecast the time-series of hospitalized, recovered and dead patients with compartmental models that involve as few parameters as possible in order to infer them solely from the data. In this regard, the model involving the least number of parameters is probably the SIR model [4] which is based on a partition of the population into:

- Uninfected people, called susceptible (S),
- Infected and contagious people (I), with more or less marked symptoms,

- People removed (R) from the infectious process, either because they are cured or unfortunately died after being infected.

If N denotes the total population that we assume to be constant over a certain time interval $[0, T]$, we have

$$N = S(t) + I(t) + R(t), \forall t \in [0, T],$$

and the evolution from S to and from I to R is given for all $t \in [0, T]$ by

$$\begin{aligned} \frac{dS}{dt}(t) &= -\frac{\beta I(t)S(t)}{N} \\ \frac{dI}{dt}(t) &= \frac{\beta I(t)S(t)}{N} - \gamma I(t) \\ \frac{dR}{dt}(t) &= \gamma I(t). \end{aligned}$$

The SIR model has only two parameters:

- $\gamma > 0$ represents the recovery rate. In other words, its inverse γ^{-1} can be interpreted as the length (in days) of the contagious period.
- $\beta > 0$ is the transmission rate of the disease. It essentially depends on two factors: the characteristics of the disease (e.g., how contagious it is) and the contact rate within the population. The larger this second parameter is, the faster the transition from susceptible to infectious will be. As a consequence, the number of hospitalized patients may increase very fast, and may lead to a collapse of the health system. Strong distancing measures like confinement can effectively act on this parameter, helping to keep it low.

Our forecasting strategy is motivated by the following observation: by allowing the parameters β and γ to be time-dependent, then we can find optimal coefficients $\beta^*(t)$ and $\gamma^*(t)$ that exactly fit any series of hospitalized and removed patients. In other words, we can perfectly fit any observed health series with a SIR model with time-dependent coefficients.

As we explain later on in the paper, the high fitting power stems from the fact that the parameters β and γ are searched in $L^\infty([0, T], \mathbb{R}_+)$, the space of essentially bounded measurable functions. For our forecasting purposes, this space is however too large to give any predictive power and we need to find a smaller manifold that has simultaneously good fitting and forecasting properties. To this aim, we develop a method based on model order reduction. The idea is to find a space of reduced complexity that can host the dynamic of the current epidemic. This reduced space is learnt from a series of detailed compartmental models based on precise underlying mechanisms of the disease. One major difficulty in these models is to fit the correct parameters. Here we use a large range of possible parameters that allow us to a large number of simulate virtual epidemic on a longer range than the fitting window $[0, T]$. We associate to each virtual epidemics of this family the time dependant parameters β and γ . The set of all such β (resp. γ) is then condensed into a reduced basis of small dimension that offers the frame for approximating the coefficients β (resp. γ) of the current epidemics, fitted on the fitting window $[0, T]$ as a linear combination of the reduced basis that, because these reduced basis are defined over a longer time range $[0, T + \tau]$ with $\tau > 0$ (say, e.g., two weeks) allows to forecast an epidemiological scenario. Its accuracy will be related to the pertinence of the mechanistic mathematical models that have been used in the learning process. All virtual simulations are considered equally important on a first stage and the procedure automatically learns what are the best scenarios (or linear combinations of scenarios) to describe the available data. The approach can even mix different models to accommodate these available data. This is contrast to other existing approaches which introduce a strong a priori belief on the quality of a certain particular model.

The paper is organized as follows. In Section 2, we present the forecasting method in the case of one single region with constant population. For this, we briefly introduce in Section 2.1 the epidemiological models involved in the procedure, namely the SIR model with time-dependent coefficients and more detailed compartmental models used for the training step. In Section 2.2, after proving that SIR models with time-dependent coefficients in $L^\infty([0, T], \mathbb{R})$ have perfect fitting properties, we present the main steps of the forecasting method. The method involves a collapsing step from detailed models to SIR models with time-dependent coefficients, and applying model reduction techniques. We detail these points in Sections 2.3 and 2.4. In Section 3 we explain that the method can easily be extended to a multi-regional context involving population mobility, and regional health data observations (provided, of course, that mobility data is available). As we explain in Section 3.1, the nature of the mobility data will dictate the kind of multi-regional SIR model to use in this context. In Section 3.2 we outline how to adapt the main steps of the method to the multi-regional case. Finally, in Section 4, we present numerical results for the period of the first pandemic wave of COVID-19 in France, which has taken place approximately between February and May 2020.

2 Methodology for one single region

For the sake of clarity, we first consider the case of one single region with constant population and no population exchange with other regions. Here, the term region is generic and may be applied to very different geographical scales, ranging from a full country, to a department within the country, or even smaller partitions of a territory.

2.1 Compartmental models

The final output of our method is a mono-regional SIR model with time dependent coefficients. It will be computed with reduced modelling techniques involving models with finer compartments with constant coefficients. Before presenting the method in the next section, we introduce here all the models along with useful notations for the rest of the paper.

SIR models with time-dependent parameters: We will fit and forecast the series of hospitalized and removed patients from hospitals (dead and recovered) with SIR models where the coefficients β and γ are time-dependent,

$$\begin{aligned}\frac{dS}{dt}(t) &= -\frac{\beta(t)I(t)S(t)}{N} \\ \frac{dI}{dt}(t) &= \frac{\beta(t)I(t)S(t)}{N} - \gamma(t)I(t) \\ \frac{dR}{dt}(t) &= \gamma(t)I(t).\end{aligned}$$

In the following, we use bold-faced letters for past-time quantities. For example, $\mathbf{f} := \{f(t) : 0 \leq t \leq T\}$ for any function $\mathbf{f} \in L^\infty([0, T], \mathbb{R})$. Using this notation, for any given β and $\gamma \in L^\infty([0, T], \mathbb{R})$ we denote by

$$(\mathbf{S}, \mathbf{I}, \mathbf{R}) = \text{SIR}(\beta, \gamma, [0, T])$$

the solution of the associated SIR dynamics in $[0, T]$.

Detailed compartmental models: Models involving many compartments offer a detailed description of epidemiological mechanisms at the expense of involving many parameters. In our approach, we use them to generate virtual scenarios. One of the initial motivations behind the present work is to provide forecasts for the Covid-19 pandemic, thus we have selected the two following models which are specific for this disease, but note that any other model could also be used.

- **First model, SEI5CHRD:** This model is inspired from the one proposed in [2]. It involves 11 different compartments and a set of 19 parameters. The dynamics of the model is illustrated in Figure 1 and the set of equations is

$$\begin{aligned}
\frac{dS}{dt}(t) &= -\frac{1}{N}S(t) (\beta_p I_p(t) + \beta_a I_a(t) + \beta_{ps} I_{ps}(t) + \beta_{ms} I_{ms}(t) + \beta_{ss} I_{ss}(t) + \beta_H H(t) + \beta_C C(t)) \\
\frac{dE}{dt}(t) &= \frac{1}{N}S(t) (\beta_p I_p(t) + \beta_a I_a(t) + \beta_{ps} I_{ps}(t) + \beta_{ms} I_{ms}(t) + \beta_{ss} I_{ss}(t) + \beta_H H(t) + \beta_C C(t)) - \varepsilon E(t) \\
\frac{dI_p}{dt}(t) &= \varepsilon E(t) - \mu_p I_p(t) \\
\frac{dI_a}{dt}(t) &= p_a \mu_p I_p(t) - \mu I_a(t) \\
\frac{dI_{ps}}{dt}(t) &= p_{ps} (1 - p_a) \mu_p I_p(t) - \mu I_{ps}(t) \\
\frac{dI_{ms}}{dt}(t) &= p_{ms} (1 - p_a) \mu_p I_p(t) - \mu I_{ms}(t) \\
\frac{dI_{ss}}{dt}(t) &= p_{ss} (1 - p_a) \mu_p I_p(t) - \mu I_{ss}(t) \\
\frac{dC}{dt}(t) &= p_c \mu I_{ss}(t) - (\lambda_{C,R} + \lambda_{C,D}) C(t) \\
\frac{dH}{dt}(t) &= (1 - p_c) \mu I_{ss}(t) - (\lambda_{H,R} + \lambda_{H,D}) H(t) \\
\frac{dR}{dt}(t) &= \lambda_{C,R} C(t) + \lambda_{H,R} H(t) \\
\frac{dD}{dt}(t) &= \lambda_{C,D} C(t) + \lambda_{H,D} H(t)
\end{aligned}$$

The different parameters involved in the model are described in Table 1 and detailed in the appendix of [2].

We denote by

$$\begin{aligned}
(\mathbf{S}, \mathbf{E}, \mathbf{I}_p, \mathbf{I}_a, \mathbf{I}_{ps}, \mathbf{I}_{ms}, \mathbf{I}_{ss}, \mathbf{C}, \mathbf{H}, \mathbf{R}, \mathbf{D}) &= \text{SEI5CHRD}(\beta_p, \beta_a, \beta_{ps}, \beta_{ms}, \beta_{ss}, \beta_H, \beta_C, \\
&\varepsilon, \mu_p, p_a, \mu, p_{ps}, p_{ms}, p_{ss}, p_c, \\
&\lambda_{CR}, \lambda_{CD}, \lambda_{HR}, \lambda_{HD}, [0, T])
\end{aligned}$$

the parameter to solution map.

- **Second model, SE2IUR:** This model is a variant of the one proposed in [5]. It involves 5 different compartments and a set of 6 parameters. The dynamics of the model is illustrated in Figure 2 and the set of equations is

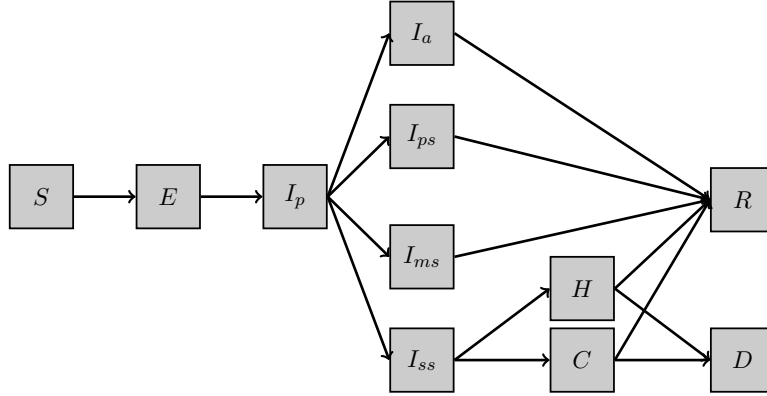


Figure 1: Model SEI5CHRD

Parameter	Description
β_p	Relative infectiousness of I_p
β_a	Relative infectiousness of I_a
β_{ps}	Relative infectiousness of I_{ps}
β_{ms}	Relative infectiousness of I_{ms}
β_{ss}	Relative infectiousness of I_{ss}
β_H	Relative infectiousness of I_H
β_C	Relative infectiousness of I_C
ε^{-1}	Latency period
μ_p^{-1}	Duration of prodromal phase
p_a	Probability of being asymptomatic
μ^{-1}	Infectious period of $I_a, I_{ps}, I_{ms}, I_{ss}$
p_{ps}	If symptomatic, probability of being paucisymptomatic
p_{ms}	If symptomatic, probability of developing mild symptoms
p_{ss}	If symptomatic, probability of developing severe symptoms
p_C	If severe symptoms, probability of going in C (note that $p_{ps} + p_{ms} + p_{ss} + p_C = 1$)
λ_{CR}	If in C, daily rate entering in R
λ_{CD}	If in C, daily rate entering in D
λ_{HR}	If hospitalized, daily rate entering in R
λ_{HD}	If hospitalized, daily rate entering in D

Table 1: Description of the parameters involved in Model SEI5CHRD

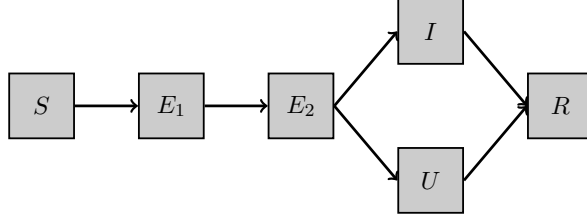


Figure 2: Model SE2IUR

Parameter	Description
β	Relative infectiousness of I, U, E_2
δ^{-1}	Latency period
σ^{-1}	Duration of prodromal phase
ν	Proportion of I among $I + U$
γ_1	If I , daily rate entering in R
γ_2	If U , daily rate entering in R

Table 2: Description of the parameters involved in Model SE2IUR

$$\begin{aligned}
 \frac{dS}{dt}(t) &= -\frac{1}{N}\beta S(t)(E_2(t) + U(t) + I(t)) \\
 \frac{dE_1}{dt}(t) &= \frac{1}{N}\beta S(t)(E_2(t) + U(t) + I(t)) - \delta E_1(t) \\
 \frac{dE_2}{dt}(t) &= \delta E_1(t) - \sigma E_2(t) \\
 \frac{dI}{dt}(t) &= \nu\sigma E_2(t) - \gamma_1 I(t) \\
 \frac{dU}{dt}(t) &= (1 - \nu)\sigma E_2(t) - \gamma_2 U(t) \\
 \frac{dR}{dt}(t) &= \gamma_1 I(t) + \gamma_2 U(t)
 \end{aligned}$$

We denote by

$$(\mathbf{S}, \mathbf{E1}, \mathbf{E2}, \mathbf{I}, \mathbf{U}, \mathbf{R}) = \text{SE2IUR}(\beta, \delta, \sigma, \nu, \gamma_1, \gamma_2, [0, T])$$

the parameter to solution map. The different parameters involved in the model are described in Table 2

- **Generalization:** In the following, we abstract the procedure as follows. For a any Detailed_Model with d compartments involving a vector $\mu \in \mathbb{R}^p$ of p parameters, we denote by

$$\mathbf{u} = \text{Detailed_Model}(\mu, [0, T]), \quad \mathbf{u} \in L^\infty([0, T], \mathbb{R})^d.$$

the parameter to solution map.

2.2 Forecasting based on model reduction of detailed models

We assume that we are given health data in a time window $[0, T]$, where $T > 0$ is assumed to be the present time. The observed data is the series of hospitalized people, denoted I_d , and people sent home or dead, denoted R_d . They are usually given at a national or a regional scale and on a daily basis. For our discussion, it will be useful to work with time-continuous functions and $t \rightarrow I_d(t)$ will denote the piecewise constant approximation in $[0, T]$ from the given data (and similarly for $R_d(t)$). Our goal is to give short-term forecasts of the series in a time window $\tau > 0$ whose size will be about two weeks. We denote by $I(t)$ and $R(t)$ the approximations to the series $I_d(t)$ and $R_d(t)$ at any time $t \in [0, T + \tau]$.

As already brought up, we propose to fit the data and provide forecasts with SIR models with time-dependent parameters β and γ . The main motivation for using such a simple family is because it possesses optimal fitting and forecasting properties for our purposes in the sense that we explain next. Defining the cost function

$$\mathcal{J}(\beta, \gamma, [0, T]) = \int_0^T (|I(t) - I_d(t)|^2 + |R(t) - R_d(t)|^2) dt \quad \text{such that } (\mathbf{S}, \mathbf{I}, \mathbf{R}) = \text{SIR}(\beta, \gamma, [0, T]),$$

the fitting problem can be expressed at the continuous level as the optimal control problem of finding

$$J^* = \inf_{(\beta, \gamma) \in L^\infty([0, T], \mathbb{R}) \times L^\infty([0, T], \mathbb{R})} \mathcal{J}(\beta, \gamma, [0, T]). \quad (1)$$

The following result ensures the existence of a unique minimizer under very mild constraints.

Proposition 2.1. *Let $N \in \mathbb{N}^*$ and $T > 0$. For any real-valued functions S_d, I_d, R_d defined on $[0, T]$ satisfying*

- (i) $S_d(t) + I_d(t) + R_d(t) = N$ for every $t \in [0, T]$,
- (ii) S_d in nonincreasing on $[0, T]$,
- (iii) R_d is nondecreasing on $[0, T]$,

there exists a unique minimizer (β^*, γ^*) to problem (2.2).

Proof. One can set

$$\begin{cases} \beta^*(t) & := -\frac{N}{I_d(t)S_d(t)} \frac{dS_d(t)}{dt} \\ \gamma^*(t) & := \frac{1}{I_d(t)} \frac{dR_d}{dt}(t) \end{cases} \quad (2)$$

or equivalently

$$\begin{cases} \beta^*(t) & := -\frac{N}{I_d(t)S_d(t)} \frac{dS_d(t)}{dt} \\ \gamma^*(t) & := \frac{1}{I_d(t)} \left[\frac{dI_d}{dt}(t) - \frac{\beta(t)I_d(t)S_d(t)}{N} \right] \end{cases}$$

so that

$$(\mathbf{S}_d, \mathbf{I}_d, \mathbf{R}_d) = \text{SIR}(\beta^*, \gamma^*, [0, T])$$

and

$$\mathcal{J}(\beta^*, \gamma^*, [0, T]) = 0$$

which obviously implies that $J^* = 0$. □

This simple observation means that there exists a time-dependent SIR model which can perfectly fit the data of any epidemiological scenario that satisfies properties (i), (ii) and (iii). In particular, we can perfectly fit the series of hospitalized people with a time-dependent SIR model. Since the health data are usually given on a daily basis, we can approximate β^*, γ^* by approximating the derivatives by classical finite differences in equation (2.2).

The fact that we can build β^* and γ^* such that $\mathcal{J}(\beta^*, \gamma^*) = J^* = 0$ implies that the family of time-dependent SIR models is rich enough not only to fit the evolution of any epidemiological series, but also to deliver perfect predictions of the health data. However, this great approximation power comes at the cost of defining the parameters β and γ in $L^\infty([0, T], \mathbb{R})$ which is a space that is too large in order to be able to define any interpretable quantity of any feasible prediction strategy.

In order to pin down a smaller manifold where these parameters may vary without sacrificing much on the fitting and forecasting power, our strategy is as follows:

1. Learning phase:

(a) Generate virtual scenarios using detailed models with constant coefficients:

- Define the notion of `Detailed_Model` which is most appropriate for the epidemiological study. Several models could be considered. For our numerical application, the detailed models were defined in Section 2.1.
- Define an interval range $\mathcal{P} \subset \mathbb{R}^p$ where the parameters μ of `Detailed_Model` will vary and draw $K \gg 1$ instances $\mu_1, \dots, \mu_K \in \mathcal{P}$.
- Compute $\mathbf{u}_i = \text{Detailed_Model}(\mu_i, [0, T + \tau])$ for $i \in \{1, \dots, K\}$. Each \mathbf{u}_i is a virtual epidemiological scenario. An important detail for our prediction purposes is that the simulations are done in $[0, T + \tau]$, that is, we simulate not only in the fitting time interval but also in the prediction time interval.

(b) **Collapse:** For every $i \in \{1, \dots, K\}$, collapse the detailed models \mathbf{u}_i into a SIR model following the ideas which we explain in Section 2.3. For every i , the procedure gives time-dependent parameters β_i and γ_i and associated SIR solutions $(\mathbf{S}_i, \mathbf{I}_i, \mathbf{R}_i)$ in $[0, T + \tau]$.

(c) **Compute reduced models:** We apply model reduction techniques using $\{\beta_i\}_{i=1}^K$ and $\{\gamma_i\}_{i=1}^K$ as training sets in order to build two basis

$$B_n = \text{span}\{b_1, \dots, b_n\}, \quad G_n = \text{span}\{g_1, \dots, g_n\} \subset L^\infty([0, T + \tau], \mathbb{R}),$$

which are defined over $[0, T + \tau]$. We outline in Section 2.4 the methods that have been explored in our numerical tests.

2. **Fitting on the reduced spaces:** We next solve the fitting problem (2.3) in the interval $[0, T]$ by searching β and γ in B_n and G_n instead of in $L^\infty([0, T], \mathbb{R})$, that is,

$$J_{(B_n, G_n)}^* = \min_{(\beta, \gamma) \in B_n \times G_n} \mathcal{J}(\beta, \gamma, [0, T]). \quad (3)$$

Obviously, since B_n and $G_n \subset L^\infty([0, T], \mathbb{R})$, we have that

$$J^* \leq J_{(B_n, G_n)}^*,$$

but we numerically observe that $J_{(B_n, G_n)}^* \rightarrow J^*$ very rapidly as $n \rightarrow \infty$, which indirectly confirms the fact that the manifold generated by the two above models accommodates well the Covid-19 epidemics.

The solution of problem (2) gives us coefficients $(c_i^*)_{i=1}^n$ and $(\tilde{c}_i^*)_{i=1}^n \in \mathbb{R}^n$ such that the time-dependent parameters

$$\begin{aligned}\beta_n^*(t) &= \sum_{i=1}^n c_i^* b_i(t), \quad \forall t \in [0, T + \tau], \\ \gamma_n^*(t) &= \sum_{i=1}^n \tilde{c}_i^* g_i(t).\end{aligned}$$

attain the minimum (2).

3. **Forecast:** For a given dimension n of the reduced spaces, propagate in $[0, T + \tau]$ the associated SIR model

$$(\mathbf{S}_n^*, \mathbf{I}_n^*, \mathbf{R}_n^*) = \text{SIR}(\beta^*, \gamma^*, [0, T + \tau])$$

The values $I_n^*(t)$ and $R_n^*(t)$ for $t \in [T, T + \tau]$ are then used for prediction.

4. **Forecast Combination/Aggregation of Experts (optional step):** By varying the dimension n and using different model reduction approaches, we can easily produce a collection of different forecasts and the question of how to select the best predictive model arises. Alternatively, instead of searching for a “best” model, one can also resort to Forecast Combination techniques [7]. Denoting $(I_1, R_1), \dots, (I_K, R_K)$ the different forecasts, the idea is to search for an appropriate linear combination

$$I^C(t) = \sum_{i=1}^K w_k I_k(t)$$

and similarly for R . Note that these combinations do not need to involve forecasts from our methodology only but other approaches like time series forecasts could also be included. One simple forecast combination is the average, in which all alternative forecasts are given the same weight $w_k = 1/K$, $k = 1, \dots, K$. More elaborate approaches consist in estimating the weights that minimize a loss function involving the forecast error.

Before going into the details of some of the steps, two remarks are in order:

1. To bring out the essential mechanisms, we have idealized some elements in the above discussion by omitting certain unavoidable discretization aspects. To start with, the ODE solutions cannot be computed exactly but only up to some accuracy given by a numerical integration scheme. In addition, the optimal control problems (2.3) and (2) are non-convex. As a result, in practice we can only find a local minima. Note however that modern solvers find solutions which are very satisfactory for all practical purposes. In addition, note that solving the control problem in a reduced space as in (2) could be interpreted as introducing a regularizing effect with respect to the control problem (2.3) in the full $L^\infty([0, T], \mathbb{R})$ space. It is to be expected that the search of global minimizers is facilitated in the reduced landscape.
2. Some numerical experiments motivated us to implement a variant of problem (2) where we consider the cost function

$$\tilde{\mathcal{J}}(\beta, \gamma, [0, T]) = \int_0^T (|\beta - \beta_n^*|^2 + |\gamma - \gamma_n^*|^2) dt \quad \text{such that } (\mathbf{S}, \mathbf{I}, \mathbf{R}) = \text{SIR}(\beta, \gamma, [0, T]).$$

In other words, we extrapolate the profiles fitted on $[0, T]$ to the future time domain $[T, \tau]$. This means that we search for coefficients c_i^* such that the fitted profiles coincide as much as possible on $[0, T]$. In Section 4, we will refer to the standard fitting method as **routine-IR** and to this variant as **routine- $\beta\gamma$** .

2.3 Details on Step 1-(b): Collapsing the detailed models into SIR dynamics

This step aims at collapsing the results of a detailed model $\mathbf{u}_i \in L^\infty([0, T + \tau], \mathbb{R}^d)$ where d is possibly large ($d = 11$ in the case of SEI5CHRD model and $d = 5$ in the case of SE2IUR's one) into a SIR model (where $d = 3$) with time-dependent parameters β_i and γ_i . For each $i \in \{1, \dots, K\}$, the d compartment profiles of \mathbf{u}_{μ_i} are reorganized into only three profiles $\mathbf{S}_i^{\text{collapse}}$, $\mathbf{I}_i^{\text{collapse}}$ and $\mathbf{R}_i^{\text{collapse}}$. More precisely, for SEI5CHRD model, this is done as follows

$$\begin{aligned}\mathbf{S}_i^{\text{collapse}} &= \mathbf{S}_i + \mathbf{E}_i \\ \mathbf{I}_i^{\text{collapse}} &= \mathbf{I}_{p_i} + \mathbf{I}_{a_i} + \mathbf{I}_{ps_i} + \mathbf{I}_{ms_i} + \mathbf{I}_{ss_i} + \mathbf{C}_i + \mathbf{H}_i \\ \mathbf{R}_i^{\text{collapse}} &= \mathbf{R}_i + \mathbf{D}_i\end{aligned}$$

and for SE2IUR's one, the collapsing writes

$$\begin{aligned}\mathbf{S}_i^{\text{collapse}} &= \mathbf{S}_i + \mathbf{E}_{1i} \\ \mathbf{I}_i^{\text{collapse}} &= \mathbf{E}_{2i} + \mathbf{I}_i + \mathbf{U}_i \\ \mathbf{R}_i^{\text{collapse}} &= \mathbf{R}_i\end{aligned}$$

Once the collapsed variables are obtained, the time-dependent parameters β_i and γ_i of the SIR model can be identified through the fitting procedure given by Equation (2.3) where the time domain is $[0, T + \tau]$ and where the profiles $\mathbf{I}_i^{\text{collapse}}$ and $\mathbf{R}_i^{\text{collapse}}$ play the role of I_d and R_d in Equation (2.3). For the sake of clarity, we write the problem applied to the current context. For any $(\beta, \gamma) \in L^\infty([0, T + \tau], \mathbb{R}) \times L^\infty([0, T + \tau], \mathbb{R})$, we consider the cost function

$$\mathcal{J}_i(\beta, \gamma) = \int_0^{T+\tau} \left(|I(t) - I_i^{\text{collapse}}(t)|^2 + |R(t) - R_i^{\text{collapse}}(t)|^2 \right) dt$$

with

$$(\mathbf{S}, \mathbf{I}, \mathbf{R}) = \text{SIR}(\beta, \gamma, [0, T + \tau]),$$

and then solve the optimization problem

$$(\beta_i, \gamma_i) \in \underset{(\beta, \gamma) \in L^\infty([0, T+\tau], \mathbb{R}) \times L^\infty([0, T+\tau], \mathbb{R})}{\text{arg inf}} \mathcal{J}_i(\beta, \gamma, [0, T + \tau]). \quad (4)$$

Note that the problem has a very simple solution since it suffices to apply formula (2.2) for solving it.

Repeating this procedure for every scenario $i \in \{1, \dots, K\}$ yields two families of time-dependent functions $\{\beta_i\}_{i=1}^K$ and $\{\gamma_i\}_{i=1}^K$ defined on the interval $[0, T + \tau]$.

2.4 Details on Model Order Reduction

Model Order Reduction is a family of methods aiming at approximating a set of solutions of parametrized PDEs or ODEs (or related quantities) with linear spaces, which are called reduced models or reduced spaces. In our case, the sets to approximate are

$$\mathbf{B} = \{\beta(\mu) : \mu \in \mathcal{P}\} \quad \text{and} \quad \Gamma = \{\gamma(\mu) : \mu \in \mathcal{P}\},$$

where each μ is the vector of parameters of the detailed model which take values over \mathcal{P} , and $\beta(\mu)$ and $\gamma(\mu)$ are the associated time-dependent coefficients of the collapsed SIR evolution. In the following, we view \mathbf{B} and Γ are subsets of $L^2([0, T])$, and we denote $\|\cdot\|$ and $\langle \cdot, \cdot \rangle$ its

norm and inner product. This inclusion is possible since B and $\Gamma \subset L^\infty([0, T], \mathbb{R})$ in view of Proposition 2.1, and $L^\infty([0, T], \mathbb{R}) \subset L^2([0, T])$ since $T < \infty$.

Let us carry the discussion for B (the same will hold for Γ). If we measure performance in terms of the worst error in the set B , the best possible performance that reduced models of dimension n can achieve is given by the Kolmogorov n -width

$$d_n(B)_{L^2([0, T])} := \inf_{\substack{Y \in L^2([0, T]) \\ \dim(Y) = n}} \max_{u \in B} \|u - P_Y u\|$$

where P_Y is the orthogonal projection onto Y . In the case of measuring errors in an average sense, the benchmark is given by

$$\delta_n(B, \nu)_{L^2([0, T])} := \inf_{\substack{Y \in L^2([0, T]) \\ \dim(Y) = n}} \int_{\mathcal{P}} \|u(y) - P_Y u(y)\| d\nu(y)$$

where ν is a probability measure on \mathcal{P} .

In practice, building spaces that meet these benchmarks is not possible. However, it is possible to build spaces whose decay is comparable to the one given by $(d_n(B)_{L^2([0, T])})_n$ or $(\delta_n(B)_{L^2([0, T])})_n$. As a result, when the Kolmogorov width decays fast, the constructed reduced spaces will deliver a very good approximation of the set B with few modes.

We next present the reduced models that we have used in our numerical experiments. Other methods could of course be considered. We carry the discussion in a fully discrete setting in order to simplify the presentation and keep it as close to the practical implementation as possible. All the claims below could be written in a fully continuous sense at the expense of introducing additional mathematical objects such as certain Hilbert-Schmidt operators to define the continuous version of the SVD.

We build the reduced models using two discrete training sets of functions $\{\beta_i\}_{i=1}^K$ and $\{\gamma_i\}_{i=1}^K$ from B and Γ . The sets have been generated in step 1-(b) of our general pipeline (see Section 2.2). We consider a discretization of the time interval $[0, T + \tau]$ into a set of $Q \in \mathbb{N}^*$ points as follows $\{t_0 = 0, \dots, t_P = T, \dots, t_Q = T + \tau\}$ where $P < Q$. Thus, we can represent each function β_i as a vector of Q values

$$\beta_i = (\beta_i(t_0), \dots, \beta_i(t_Q))^T \in \mathbb{R}_+^Q.$$

and hence assemble all the functions of the family $\{\beta_i\}_{i=1}^K$ into a matrix $\mathcal{B} \in \mathbb{R}_+^{Q \times K}$. The same remark applies for the family $\{\gamma_i\}_{i=1}^K$ that gives a matrix $\mathcal{G} \in \mathbb{R}_+^{Q \times K}$.

1. **SVD:** The eigenvalue decomposition of the correlation matrix $\mathcal{B}^T \mathcal{B} \in \mathbb{R}^{K \times K}$ is

$$\mathcal{B}^T \mathcal{B} = \mathcal{V} \mathcal{D} \mathcal{V}^T,$$

where $\mathcal{V} = (v_{i,j}) \in \mathbb{R}^{K \times K}$ is an orthogonal matrix and $\mathcal{D} \in \mathbb{R}^{K \times K}$ is a rectangular diagonal matrix with non-negative entries which we denote λ_i and order them in decreasing order. The ℓ^2 -orthogonal basis functions $\{h_1, \dots, h_K\}$ are then given by the linear combinations

$$h_i = \sum_{j=1}^K v_{j,i} \beta_j, \quad 1 \leq i \leq K.$$

The space

$$B_n = \text{span}\{h_1, \dots, h_n\}$$

is the best n -dimensional space to approximate the set $\{\beta_i\}_{i=1}^K$ in the average sense. We have

$$\delta_n(\{\beta_i\}_{i=1}^K)_{\ell_2} = \left(\frac{1}{K} \sum_{i=1}^K \|\beta_i - P_{B_n} \beta_i\|_{\ell_2}^2 \right)^{-1/2} = \left(\sum_{i>n} \lambda_i \right)^{-1/2}$$

and the average approximation error is given by the sum of the tail of the eigenvalues.

Therefore the SVD method is particularly efficient if there is a fast decay of the eigenvalues, meaning that the set $\{\beta_i\}_{i=1}^K$ can be approximated by only few modes. However, note that by construction, this method does not ensure positivity in the sense that $P_{B_n} \beta_i(t)$ may become negative for some $t \in [0, T]$ although the original function $\beta_i(t) \geq 0$ for all $t \in [0, T]$. This is due to the fact that the eigenvectors h_i are not necessarily nonnegative. As we will see later, in our study, ensuring positivity especially for extrapolation (i.e., forecasting) is particularly important, and motivates the next methods.

2. **Non-negative Matrix Factorization** (NMF, see [6, 3]): NMF is a variant of SVD involving nonnegative modes and expansion coefficients. In this approach, we build a family of non-negative functions $\{\beta_i\}_{i=1}^n$ and we approximate each β_i with a linear combination

$$\beta_i^{\text{NMF}} = \sum_{j=1}^n \omega_{i,j} \mathbf{b}_j, \quad 1 \leq i \leq K, \quad (5)$$

where for every $1 \leq i \leq K$ and $1 \leq j \leq n$, the coefficients $\omega_{i,j} \geq 0$ and the basis function $\mathbf{b}_j \geq 0$. In other words, we solve the following optimization problem

$$(W, B) \in \underset{(W, B) \in \mathbb{R}_+^{K \times n} \times \mathbb{R}_+^{n \times Q}}{\arg \min} \|\mathcal{B} - WB\|_F^2.$$

We refer to [3] for further details on the NMF and its numerical aspects.

3. **Greedy algorithm with projection on an extended cone of positive functions (positive greedy)**: This method stems from the observation that NMF approximates functions in the cone of positive functions of $\text{span}\{\mathbf{b}_i \geq 0\}_{i=1}^n$ since it imposes that $\omega_{i,j} \geq 0$. We then remark that the positivity of the linear combination (2) is not equivalent to the positivity of the coefficients $\omega_{i,j}$ since there are obviously linear combinations involving very small $\omega_{i,j} < 0$ for some j which may still deliver a nonnegative linear combination $\sum_{j=1}^n \omega_{i,j} \mathbf{b}_j$.

In order to widen the cone of linear combinations and include these non negative functions, we start from a classical greedy algorithm then we iteratively propose new nonnegative basis function that we construct from the training set. The basis functions are then modified by adding a negative linear combination of the other basis functions. The coefficients are chosen in an optimal way to ensure the positivity of the final linear combination while minimizing the L^∞ -norm of the each linear combination.

We solve this problem of optimal selection of coefficients by a minimization algorithm based on an alternating directions where we define the negative coefficients e.g. as follows:

After the n^{th} stage of a classical greedy algorithm let $\varphi_1 = \beta(\mu_1), \dots, \varphi_n = \beta(\mu_n)$ (resp. $\varphi_1 = \gamma(\mu_1), \dots, \varphi_n = \gamma(\mu_n)$) be the associated reduced basis.

→ Algorithm

loop in i

$$\forall k \neq i, \quad \sigma_k^i = 0$$

loop in $\ell \neq i$

$$\alpha_\ell^{i,*} = \operatorname{argmax}\{\alpha | [\varphi_i - \sum_{k \neq \{i\}} \sigma_k^i \varphi_k - \alpha \varphi_\ell](x) > 0, \forall x\}$$

$$\sigma_\ell^i = \sigma_\ell^i + \frac{\alpha_\ell^{i,*}}{2}$$

continue until $\alpha_\ell^{i,*} \leq \text{tol}$ for all ℓ where "tol" is some (small) tolerance.

The new basis is then the function

$$\psi_i = \varphi_i - \sum_{k \neq \{i\}} \sigma_k^i \varphi_k$$

and the approximation is sought as

$$\beta_i^{PG} = \sum_{j=1}^n \omega_{i,j} \psi_j, \quad 1 \leq i \leq K,$$

with nonnegative coefficients $\omega_{i,j}$

It should be noted that if we work with positive functions that are upper bounded by a constant $L > 0$, we can ensure that the approximations, written as a linear combination of basis functions, will also be between these bounds 0 and L by defining, on the one hand and as we have just done, a cone of positive functions generated by the above family $\{\psi_i\}_i$, and, on the other hand, by considering the base of the functions $L - \varphi$, φ being as above the set all greedy elements of the reduced basis to which we also apply an enlargement of these positive functions. We then impose that the approximation is written as a positive combination of the first (positive) functions and that $L - \Psi$ (Ψ being the approximation) is also written as a combination with positive components in the second basis.

In this frame, the approximation appears under the form of a least square approximation with $2n$ linear constraints on the n coefficients expressing the fact that in the two above transformed basis the coefficients are nonnegative.

4. **Reduced models on $I = \{\mathbf{I}(\mu) : \mu \in \mathcal{P}\}$ and $R = \{\mathbf{R}(\mu) : \mu \in \mathcal{P}\}$:** Instead of applying model reduction to the sets B and Γ , we can instead apply the same above techniques directly to the sets of solutions I and R of the SIR models with time-dependent coefficients in B and Γ .

3 Methodology for multiple regions including population mobility data

The forecasting method of Section 2.2 for one single region can be extended to multiple regions involving population mobility. The prediction scheme will now be based on a multiregional SIR with time-dependent coefficients. Compared to other more detailed models, its main advantage is that it reduces drastically the number of parameters to be estimated. Indeed, detailed multiregional models such as multiregional extensions of the above SEI5CHRD and SE2IUR models from Section 2.3 require a number of parameters which quickly grows with the number K of regions involved. Their calibration thus requires large amounts of data which, in addition, may be unknown, very uncertain, or not available.

The structure of this section is the same as the previous one for the case of single region. We start by introducing in Section 3.1 the multi-regional SIR model with time-dependent coefficients

and associated details models. As any multiregional model, mobility data are required as an input information, and the nature and level of detail of the available data imposes certain choices on the modelling of the multiregional SIR (as well as the other detailed models). We next present in Section 3.2 the general pipeline, in which we emphasize the high modularity of the approach.

3.1 Multi-regional compartmental models

In the spirit of fluid flow modeling, there are essentially two ways of describing mobility between regions:

- In a Eulerian description, we take the regions as fixed references for which we record incoming and outgoing travels.
- In a Lagrangian description, we follow the motion of people domiciled in a certain region and record their travels in the territory. We can expect this modeling to be more informative on the geographical spread of the disease but it comes at the cost of additional details on the people's domicile region.

Note that both descriptions hold at any coarse or fine geographical level in the sense that what we call the regions could be taken to be full countries, departments within a country, or very small geographical partitions of a territory. We next describe the multi-regional SIR models with the Eulerian and Lagrangian description of population fluxes which will be the output of our methodology.

3.1.1 Multi-regional SIR models with time-dependent parameters

Eulerian description of population flux: Assume that we have K regions and the number of people in region i is N_i . Due to mobility, the population in each region varies, so N_i depends on t . However, the total population is assumed to be constant and equal to N , that is

$$N = \sum_{i=1}^K N_i(t), \quad \forall t \geq 0.$$

For any $t \geq 0$, let $\lambda_{i \rightarrow j}(t) \in [0, 1]$ be the probability that people from i travel to j at time t . In other words, $\lambda_{i \rightarrow j}(t)N_i(t)dt$ is the number of people from region i that have travelled to region j between time t and $t + dt$. Note that we have

$$\sum_{j=1}^K \lambda_{i \rightarrow j}(t) = 1, \quad \forall t \geq 0.$$

Since, for any $dt \geq 0$,

$$N_i(t + dt) = N_i(t) - \sum_{j \neq i} \lambda_{i \rightarrow j}(t)N_i(t)dt + \sum_{j \neq i} \lambda_{j \rightarrow i}(t)N_j(t)dt$$

dividing by dt and taking the limit $dt \rightarrow 0$ yields

$$\frac{dN_i}{dt}(t) = - \sum_{j \neq i} \lambda_{i \rightarrow j}(t)N_i(t) + \sum_{j \neq i} \lambda_{j \rightarrow i}(t)N_j(t).$$

Note that we have

$$\sum_{i=1}^K \frac{dN_i}{dt}(t) = 0, \quad \forall t \geq 0.$$

Thus $\sum_i N_i(t) = \sum_i N_i(0) = N$, which is consistent with our assumption that the total population is constant.

The time evolution of the N_i is known in this case if we are given the $\lambda_{i \rightarrow j}(t)$ from Eulerian mobility data. In addition to this mobility data, we also have the data of the evolution of hospitalized, deceased and healed people and our goal is to fit a multiregional SIR model that is in accordance with this data. We propose the following model.

Denoting S_i , I_i and R_i the number of Susceptible, Infectious and Recovered people in region i at time t , we first have the relation

$$N_i(t) = S_i(t) + I_i(t) + R_i(t) \quad \Leftrightarrow \quad 1 = \frac{S_i(t)}{N_i(t)} + \frac{I_i(t)}{N_i(t)} + \frac{R_i(t)}{N_i(t)}.$$

Note that from the second relation, it follows that

$$0 = \frac{d S_i}{dt} \frac{1}{N_i} + \frac{d I_i}{dt} \frac{1}{N_i} + \frac{d R_i}{dt} \frac{1}{N_i}. \quad (6)$$

To model the evolution between compartments, one possibility is the following SIR model

$$\begin{aligned} \frac{d S_i}{dt} \frac{1}{N_i} &= - \left(\beta_i \lambda_{i \rightarrow i} \frac{I_i}{N_i} + \sum_{j \neq i} \beta_j \lambda_{j \rightarrow i} \frac{I_j}{N_j} \right) \frac{S_i}{N_i} \\ \frac{d I_i}{dt} \frac{1}{N_i} &= - \frac{d S_i}{dt} \frac{1}{N_i} - \gamma_i \frac{I_i}{N_i} \\ \frac{d R_i}{dt} \frac{1}{N_i} &= \gamma_i \frac{I_i}{N_i}, \end{aligned} \quad (7)$$

The parameters β_i , γ_i , N_i depend on t but we have omitted the dependence to ease the reading. Introducing the compartmental densities

$$s_i = \frac{S_i}{N_i}, \quad i_i = \frac{I_i}{N_i}, \quad r_i = \frac{R_i}{N_i},$$

the system equivalently reads

$$\begin{aligned} \frac{d}{dt} s_i &= - \left(\beta_i \lambda_{i \rightarrow i} i_i + \sum_{j \neq i} \beta_j \lambda_{j \rightarrow i} i_j \right) s_i \\ \frac{d}{dt} i_i &= - \frac{d}{dt} s_i - \gamma_i i_i \\ \frac{d}{dt} r_i &= \gamma_i i_i, \end{aligned} \quad (8)$$

Before going further, some comments are in order:

- The model is consistent in the sense that it satisfies (3.1.1) and when $K = 1$ we recover the traditional SIR model.
- Under lockdown measures, $\lambda_{i \rightarrow j} \approx \delta_{i,j}$ and the population $N_i(t)$ remains practically constant. As a result, the evolution of each region is decoupled from the others and each region can be addressed with the mono-regional approach.
- The use of β_j in equation (3.1.1) is debatable. When the people from region j arrive to region i , it may be reasonable to assume that the contact rate is β_i .

- The use of $\lambda_{j \rightarrow i}$ in equation (3.1.1) is also very debatable. The probability $\lambda_{j \rightarrow i}$ was originally defined to account for the mobility of people from region j to region i without specifying the compartment. However, in equation (3.1.1), we need the probability of mobility of infectious people from region j to region i , which we denote by $\mu_{j \rightarrow i}$ in the following. It seems reasonable to think that $\mu_{j \rightarrow i}$ may be smaller than $\lambda_{j \rightarrow i}$ because as soon as people become symptomatic and suspect their illness, they will probably not move. Two possible options would be:
 - We could try to make a guess on $\mu_{j \rightarrow i}$. If the symptoms arise, say, 2 days after infection and if we recover in 15 days in average, then we could say that $\mu_{j \rightarrow i} = 2/15\lambda_{j \rightarrow i}$.
 - Since, the above seems however pretty empirical, the option adopted in this work is to use $\lambda_{j \rightarrow i}$ and absorb the uncertainty in the values of the β_j that we will fit.

Lagrangian description of population flux: We call the above description Eulerian because we have fixed the departments as a fixed reference. Another point of view is to follow the trajectories of inhabitants of each region, in the same spirit as when we follow the trajectories of fluid particles.

Let now S_i , I_i , R_i the number of susceptible, infectious and recovered people who are domiciled in region i . It is reasonable to assume that $S_i(t) + I_i(t) + R_i(t)$ is constant in time. However, all the dwellers of region i may not all be in that region at time t . Let $\lambda_{j \rightarrow k}^{(i)}(t)$ be the probability that susceptible people domiciled at i travel from region j to region k at time t . With this notation, $\lambda_{i \rightarrow i}^{(i)}(t)$ is the probability that susceptible people domiciled at i remain in region i at time t . Similarly, let $\mu_{j \rightarrow k}^{(i)}(t)$ be the probability that infectious people domiciled at i travel from region j to k at time t . Hence the total number of susceptible and infectious people that are in region i at time t is

$$\begin{aligned} \mathcal{S}_i(t) &= \sum_{k=1}^K \sum_{j=1}^K \left(\lambda_{j \rightarrow i}^{(k)}(t) - \lambda_{i \rightarrow j}^{(k)}(t) \right) S_k(t) \\ \mathcal{I}_i(t) &= \sum_{k=1}^K \sum_{j=1}^K \left(\mu_{j \rightarrow i}^{(k)}(t) - \mu_{i \rightarrow j}^{(k)}(t) \right) S_k(t) \end{aligned}$$

We can thus write the evolution over S_i , I_i , R_i as

$$\begin{aligned} \frac{dS_i}{dt} &= - \sum_{j=1}^K \sum_{k=1}^K \beta_k(t) \lambda_{j \rightarrow k}^{(i)}(t) S_i(t) \mathcal{I}_k(t) \\ \frac{dI_i}{dt} &= - \frac{dS_i}{dt} - \gamma_i(t) I_i(t) \\ \frac{dR_i}{dt} &= \gamma_i(t) I_i(t) \end{aligned} \tag{9}$$

Note that $S_i(t) + I_i(t) + R_i(t)$ is constant, which is consistent with the fact that in our model

$$\frac{d}{dt}(S_i + I_i + R_i) = 0.$$

We emphasize that, to implement this model, one needs the Lagrangian mobility data $\lambda_{j \rightarrow k}^{(i)}$ for all $(i, j, k) \in \{1, \dots, K\}^3$.

Notation: In the following, we gather the compartmental variables in vectors

$$\vec{\mathbf{S}} := (\mathbf{S})_{i=1}^K, \quad \vec{\mathbf{I}} := (\mathbf{I})_{i=1}^K, \quad \vec{\mathbf{R}} := (\mathbf{R})_{i=1}^K$$

as well as the time-dependent coefficients

$$\vec{\beta} = (\beta)_{i=1}^K, \quad \vec{\gamma} = (\gamma)_{i=1}^K.$$

For any $\vec{\beta}$ and $\vec{\gamma} \in (L^\infty([0, T], \mathbb{R}))^K$, we denote by

$$(\vec{\mathbf{S}}, \vec{\mathbf{I}}, \vec{\mathbf{R}}) = \text{Multiregional_SIR}(\vec{\beta}, \vec{\gamma}, [0, T])$$

the output of any of the above multiregional SIR models.

3.1.2 Detailed multi-regional models with constant coefficients

In the spirit of the multi-regional SIR, one can formulate detailed multi-regional versions of more detailed models such as the ones introduced in Section 2.1. We omit the details for the sake of brevity.

3.2 Forecasting for multiple regions with population mobility

Similarly as in the mono-regional case, we assume that we are given health data in $[0, T]$ in all regions. The observed data in region i is the series of hospitalized people, denoted I_i^d , and people sent home or dead, denoted R_i^d . They are usually given at a national or a regional scale and on a daily basis.

We propose to fit the data and provide forecasts with SIR models with time-dependent parameters β_i and γ_i for each region i . Like in the mono-regional case, we can prove that such a simple family possesses optimal fitting properties for our purposes. In the current case, the cost function reads

$$\mathcal{J}(\vec{\beta}, \vec{\gamma}, [0, T]) = \sum_{i=1}^K \int_0^T \left(|I_i(t) - I_i^d(t)|^2 + |R_i(t) - R_i^d(t)|^2 \right) dt$$

such that $(\vec{\mathbf{S}}, \vec{\mathbf{I}}, \vec{\mathbf{R}}) = \text{Multiregional_SIR}(\vec{\beta}, \vec{\gamma}, [0, T])$,

and the fitting problem is the optimal control problem of finding

$$J^* = \inf_{\vec{\beta}, \vec{\gamma} \in (L^\infty([0, T], \mathbb{R}))^K \times (L^\infty([0, T], \mathbb{R}))^K} \mathcal{J}(\vec{\beta}, \vec{\gamma}, [0, T]). \quad (10)$$

The following proposition ensures the existence of a unique minimizer under certain conditions. To prove it, it will be useful to remark that any of the above multi-regional SIR models (see (3.1.1), (3.1.1)) can be written in the general form

$$\begin{aligned} \frac{d\vec{\mathbf{S}}}{dt} &= M(\Lambda(t), \vec{\mathbf{S}}(t), \vec{\mathbf{I}}(t)) \vec{\beta} \\ \frac{d\vec{\mathbf{I}}}{dt} &= -\frac{d\vec{\mathbf{S}}}{dt} - \text{diag}(\mathbf{I}(t)) \vec{\gamma} \\ \frac{d\vec{\mathbf{R}}}{dt} &= \text{diag}(\mathbf{I}(t)) \vec{\gamma}, \end{aligned}$$

where, by a slight abuse of notation, the vectors $\vec{\mathbf{S}}$, $\vec{\mathbf{I}}$ and $\vec{\mathbf{R}}$ are densities of population in the case of the Eulerian approach (see equation (3.1.1)). They are classical population numbers in

the case of the Lagrangian approach (see equation (3.1.1)). $\text{diag}(\mathbf{I}(t))$ is the $K \times K$ diagonal matrix with diagonal entries given by the vector $\mathbf{I}(t)$. $M(\Lambda(t), \vec{\mathbf{S}}(t), \vec{\mathbf{I}}(t))$ is a matrix of size $K \times K$ which depends on the vectors of susceptible and infectious people $\vec{\mathbf{S}}(t), \vec{\mathbf{I}}(t)$ and on the mobility matrix Λ . In the case of the Eulerian description, $\Lambda(t) = (\lambda_{i,j}(t))_{1 \leq i,j \leq K}$ and in the case of the Lagrangian approach $\Lambda(t)$ is the $K \times K \times K$ tensor $\Lambda(t) = (\lambda_{j,k}^{(i)}(t))_{1 \leq i,j,k \leq K}$. For example, in the case of the Eulerian model (3.1.1), the matrix M reads

$$M(\Lambda(t), \vec{\mathbf{S}}(t), \vec{\mathbf{I}}(t)) = -\text{diag}(\vec{\mathbf{S}}(t))\Lambda^T \text{diag}(\vec{\mathbf{I}}(t)) = -(S_i \lambda_{i \rightarrow j} I_j)_{1 \leq i,j \leq K} \quad (11)$$

Proposition 3.1. *If $M(\Lambda(t), \vec{\mathbf{S}}(t), \vec{\mathbf{I}}(t))$ is invertible for all $t \in [0, T]$, then there exists a unique minimizer $(\vec{\beta}^*, \vec{\gamma}^*)$ to problem (3.2).*

Proof. Since we assume that $M(\Lambda(t), \vec{\mathbf{S}}(t), \vec{\mathbf{I}}(t))$ is invertible for every $t \in [0, T]$, we can set

$$\begin{cases} \vec{\beta}^*(t) & := M^{-1}(t) \frac{d\vec{\mathbf{S}}}{dt} \\ \vec{\gamma}^*(t) & := \text{diag}^{-1}(I(t)) \frac{d\vec{\mathbf{R}}}{dt} \end{cases}$$

or equivalently

$$\begin{cases} \vec{\beta}^*(t) & := M^{-1}(t) \frac{d\vec{\mathbf{S}}}{dt} \\ \vec{\gamma}^*(t) & := -\text{diag}^{-1}(I(t)) \left(\frac{d\vec{\mathbf{I}}}{dt} + M(\Lambda(t), \vec{\mathbf{S}}(t), \vec{\mathbf{I}}(t)) \vec{\beta}^* \right) \end{cases}$$

so that

$$(\vec{\mathbf{S}}^d, \vec{\mathbf{I}}^d, \vec{\mathbf{R}}^d) = \text{Multiregional_SIR}(\vec{\beta}^*, \vec{\gamma}^*, [0, T])$$

and

$$\mathcal{J}(\vec{\beta}^*, \vec{\gamma}^*, [0, T]) = 0$$

which implies that $J^* = 0$. □

Before going further, let us comment on the invertibility of $M(\Lambda(t), \vec{\mathbf{S}}(t), \vec{\mathbf{I}}(t))$ which is necessary in Proposition 3.1. A sufficient condition to ensure it is if the matrix is diagonally dominant row-wise or column-wise. This yields certain conditions on the mobility matrix $\Lambda(t)$ with respect to the values of $\vec{\mathbf{S}}(t), \vec{\mathbf{I}}(t)$. For example, if M is defined as in equation (3.2), the matrix is diagonally dominant per rows if for every $1 \leq i \leq K$,

$$\lambda_{i \rightarrow i} > \sum_{j \neq i} \lambda_{i \rightarrow j} \frac{I_j}{I_i}.$$

Similarly, if for every $1 \leq j \leq K$,

$$\lambda_{j \rightarrow j} > \sum_{i \neq j} \lambda_{i \rightarrow j} \frac{S_i}{S_j},$$

then the matrix is diagonally dominant per columns, and guarantees invertibility. Note that any of the above conditions is satisfied in scenarios with little or no mobility where $\lambda_{i \rightarrow i} \approx \delta_{i,j}$.

Now that we have exactly defined the set up for the multi-regional case, we can follow the same steps of Section 2.2 to derive forecasts involving model reduction for the time-dependent variables $\vec{\beta}$ and $\vec{\gamma}$.

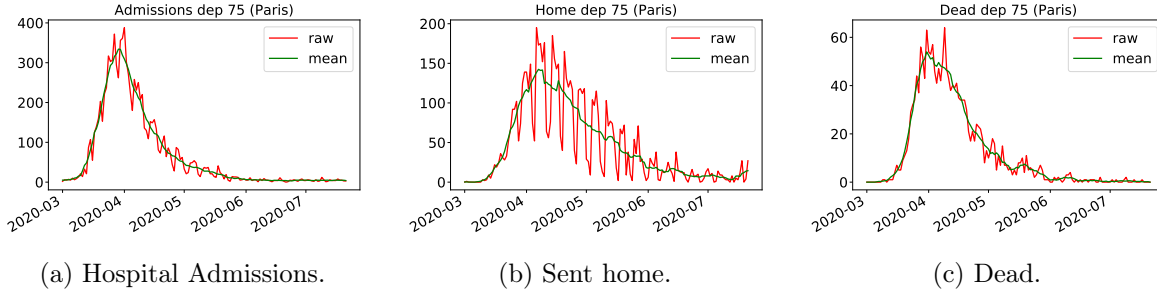


Figure 3: Paris.

4 Numerical results: the example of Paris

In this section we apply our forecasting method to the first pandemic wave of COVID-19 in France which has taken place approximately between February and May 2020. In particular, we consider the period going from March 5 to May 7, 2020. Due to the lockdown imposed between March 11 and May 11, inter-regional population mobility was drastically reduced. Studies using anonymized Facebook data have estimated the reduction in 80% (see [1]). As a result, it is reasonable to treat each region independently from the rest, and we apply the mono-regional setting of Section 2. In a forthcoming paper, we will apply the fully multi-regional setting for the post-lockdown period. We next present numerical results for the case of the Paris region, and we report the extrapolation errors obtained using the methods introduced in this paper. Forecasts will be done on a 20 days window, starting from 25/03/2020, 05/04/2020 and 15/04/2020. We will examine the accuracy by studying the relative errors for 7 and 14 days.

4.1 Health Data

We use data from the SI-VIC database to get the number $I_d(t)$ of hospitalized, and $R_d(t)$ of recovered people (sent home or dead). The database was pre-processed and made available to us by the DREES¹. As shown in Figure 3, the delivered data by DREES present sharp oscillations at the scale of the week (see red curves), which are due to administrative delays in which the cases were officially reported by the hospitals. For our methodology, we have smoothed the data by applying a 7 days moving average filter (see green curves). In order to account for the total number of infected people, we also multiply the data by an adjustment factor $\alpha = 15$ as hinted from [2]. Obviously, this factor is uncertain and could be improved in the light of further retrospective studies of the outbreak. However, note that when $S \gg I$ in the start of the epidemic, the impact of this factor is negligible in the dynamics as can be understood from (2.2).

4.2 Fitting error analysis

In this section we study the quality of fitting $\beta(t)$ and $\gamma(t)$ using the reduced bases B_n and G_n . The bases are obtained as described in the previous section using $K = 2618$ virtual scenarios generated using SE2IUR and SEI5CHRD (see steps 1 and 2 of the pipeline of Section 2.2). First we look at the eigenvalues for β and γ when performing a SVD decomposition for the virtual scenarios. Figure 4 shows a rapid decay of the eigenvalues obtained by SVD decomposition, it

¹DREES stands for Direction de la Recherche, des Études, de l'Évaluation et des Statistiques. It is a department within the Ministry of Solidarity and Health. Website: <https://drees.solidarites-sante.gouv.fr/etudes-et-statistiques/>

shows that we can obtain a good approximation with only a few modes. Let us now look at the fitting error for β and γ . The fitting procedure works both on the components of the reduced basis and the initial time of the epidemics to minimize the loss function.

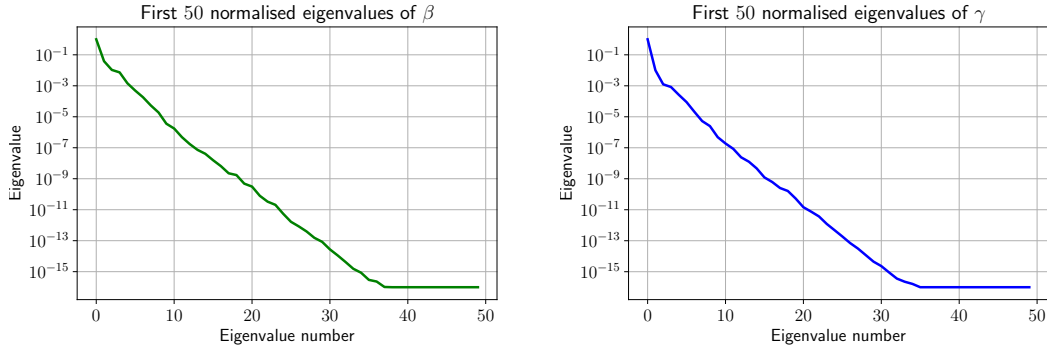


Figure 4: Eigenvalues decay

n	SVD		NMF		Greedy	
	β	γ	β	γ	β	γ
5	1.77×10^{-2}	1.76×10^{-2}	2.45×10^{-2}	2.53×10^{-1}	2.09×10^{-2}	2.20×10^{-2}
7	1.64×10^{-2}	1.54×10^{-2}	1.88×10^{-2}	1.99×10^{-1}	2.07×10^{-2}	2.21×10^{-2}
9	1.51×10^{-2}	1.45×10^{-2}	1.93×10^{-2}	1.89×10^{-1}	2.01×10^{-2}	2.41×10^{-2}
11	1.29×10^{-2}	1.03×10^{-2}	1.97×10^{-2}	1.39×10^{-1}	2.06×10^{-2}	2.04×10^{-2}
13	1.13×10^{-2}	8.17×10^{-3}	2.14×10^{-2}	6.73×10^{-2}	2.13×10^{-2}	1.99×10^{-2}
15	7.00×10^{-3}	3.67×10^{-3}	2.21×10^{-2}	4.73×10^{-2}	2.08×10^{-2}	2.26×10^{-2}
17	6.39×10^{-3}	3.62×10^{-3}	2.31×10^{-2}	1.02×10^{-1}	2.14×10^{-2}	2.34×10^{-2}

Table 3: L^1 -relative error from 15/03 to 13/04

n	SVD		NMF		Greedy	
	β	γ	β	γ	β	γ
5	1.81×10^{-2}	1.67×10^{-2}	1.99×10^{-2}	1.70×10^{-1}	2.20×10^{-2}	2.21×10^{-2}
7	1.79×10^{-2}	1.51×10^{-2}	2.05×10^{-2}	1.69×10^{-1}	2.12×10^{-2}	2.12×10^{-2}
9	1.53×10^{-2}	1.45×10^{-2}	2.20×10^{-2}	1.21×10^{-1}	2.16×10^{-2}	2.11×10^{-2}
11	1.45×10^{-2}	1.25×10^{-2}	1.91×10^{-2}	7.09×10^{-2}	2.13×10^{-2}	2.19×10^{-2}
13	1.24×10^{-2}	1.14×10^{-2}	2.16×10^{-2}	7.43×10^{-2}	2.13×10^{-2}	2.12×10^{-2}
15	9.57×10^{-3}	9.11×10^{-3}	2.02×10^{-2}	7.62×10^{-2}	2.13×10^{-2}	2.07×10^{-2}
17	8.57×10^{-3}	7.91×10^{-3}	1.98×10^{-2}	9.13×10^{-2}	2.06×10^{-2}	2.10×10^{-2}

Table 4: L^1 -relative error from 26/03 to 25/04

n	SVD		NMF		Greedy	
	β	γ	β	γ	β	γ
5	1.71×10^{-2}	1.58×10^{-2}	3.35×10^{-2}	8.14×10^{-2}	2.86×10^{-2}	3.71×10^{-2}
7	1.62×10^{-2}	1.44×10^{-2}	2.37×10^{-2}	5.72×10^{-2}	2.91×10^{-2}	3.94×10^{-2}
9	1.49×10^{-2}	1.36×10^{-2}	3.01×10^{-2}	5.75×10^{-2}	2.97×10^{-2}	4.64×10^{-2}
11	1.32×10^{-2}	1.24×10^{-2}	2.26×10^{-2}	4.47×10^{-2}	2.60×10^{-2}	3.99×10^{-2}
13	1.24×10^{-2}	1.16×10^{-2}	2.68×10^{-2}	4.01×10^{-2}	2.55×10^{-2}	3.54×10^{-2}
15	1.17×10^{-2}	1.11×10^{-2}	1.96×10^{-2}	4.54×10^{-2}	2.86×10^{-2}	4.85×10^{-2}
17	1.17×10^{-2}	8.06×10^{-3}	2.43×10^{-2}	6.30×10^{-2}	2.84×10^{-2}	5.82×10^{-2}

Table 5: L^1 -relative error from 05/04 to 05/05

We do not observe a convergence as more modes are taken into account. This is due to the noise coming from the data. The tables show that overall the fitting errors are the lowest when considering a SVD reduced basis; the Greedy approach shows lower errors than the NMF strategy which produces the highest fitting errors. These errors show how well the reduced basis can represent the data, it is the best approximations possibles that can be obtained when performing a forecast.

4.3 Forecasting error analysis

We have examined all the model reduction techniques outlined in Section 2.4:

- The **routine- $\beta\gamma$** fits and extrapolates β_n^* and γ_n^* using reduced bases B_n and G_n for the sets B and Γ (see Section 2.4). As outlined in that section, we consider three different methods to build B_n and G_n : one based on simple SVD, one based on NMF, and one based on a greedy algorithm on an extended cone of positive functions. The corresponding forecast for I and R are then solutions of the SIR model using the forecasts of $\beta(t)$ and $\gamma(t)$. For this method we choose to do the fitting on the 10 days prior to the start of the extrapolation.
- The **routine-IR** works directly on the sets $I = \{\mathbf{I}(\mu) : \mu \in \mathcal{P}\}$ and $R = \{\mathbf{R}(\mu) : \mu \in \mathcal{P}\}$. We again have three model reduction methods. For this approach we choose to do the fitting on all days (starting from 05/03/2020) prior to the start of the extrapolation.

For each method, we study the impact of the dimension n of the reduced basis.

4.3.1 Forecasting with routine- $\beta\gamma$

Table 6 shows the relative errors of a 7 days and 14 days forecast from 25/03 for each extrapolation method and each reduced basis. Similarly tables 7 and 8 show forecasts relative errors respectively from 05/04 and 15/04.

Forecast 7 days									
	SVD			NMF			Greedy		
n	$I(L^1)$	$I(L^\infty)$	$R(L^\infty)$	$I(L^1)$	$I(L^\infty)$	$R(L^\infty)$	$I(L^1)$	$I(L^\infty)$	$R(L^\infty)$
5	2.12×10^1	1.17×10^2	2.79×10^0	7.64×10^{-1}	1.71×10^0	1.61×10^{-1}	3.78×10^{-2}	9.48×10^{-2}	5.69×10^{-2}
7	1.17×10^8	7.68×10^8	1.52×10^8	3.96×10^{-1}	8.01×10^{-1}	6.15×10^{-2}	3.18×10^{-2}	6.64×10^{-2}	3.38×10^{-2}
9	∞	∞	∞	7.50×10^{-1}	1.99×10^0	2.00×10^{-1}	1.60×10^{-2}	3.53×10^{-2}	2.36×10^{-2}
11	∞	∞	∞	1.59×10^{-1}	3.38×10^{-1}	2.20×10^{-2}	2.54×10^{-1}	7.33×10^{-1}	1.22×10^{-1}
13	7.02×10^{-1}	9.61×10^{-1}	9.16×10^{-1}	3.92×10^{-1}	8.46×10^{-1}	7.19×10^{-2}	3.17×10^{-2}	6.78×10^{-2}	3.14×10^{-2}
15	∞	∞	∞	1.94×10^{-1}	4.11×10^{-1}	3.25×10^{-2}	1.35×10^{-1}	3.81×10^{-1}	8.54×10^{-2}
17	2.65×10^3	1.74×10^4	4.85×10^4	1.10×10^{-1}	2.22×10^{-1}	2.60×10^{-2}	1.50×10^{-2}	3.85×10^{-2}	2.50×10^{-2}
Forecast 14 days									
	SVD			NMF			Greedy		
n	$I(L^1)$	$I(L^\infty)$	$R(L^\infty)$	$I(L^1)$	$I(L^\infty)$	$R(L^\infty)$	$I(L^1)$	$I(L^\infty)$	$R(L^\infty)$
5	∞	∞	∞	4.83×10^0	1.60×10^1	1.91×10^0	3.09×10^{-1}	1.06×10^0	2.95×10^{-1}
7	∞	∞	∞	1.65×10^0	4.36×10^0	6.01×10^{-1}	5.28×10^{-2}	8.20×10^{-2}	4.27×10^{-2}
9	∞	∞	∞	5.16×10^1	3.75×10^2	1.62×10^1	3.21×10^{-2}	1.15×10^{-1}	2.13×10^{-2}
11	∞	∞	∞	5.46×10^{-1}	1.11×10^0	1.78×10^{-1}	1.59×10^1	1.16×10^2	7.14×10^0
13	∞	∞	∞	2.96×10^0	1.18×10^1	1.16×10^0	8.87×10^{-2}	1.33×10^{-1}	6.05×10^{-2}
15	∞	∞	∞	7.21×10^{-1}	1.64×10^0	1.82×10^{-1}	2.70×10^0	1.46×10^1	1.69×10^0
17	∞	∞	∞	2.79×10^{-1}	4.28×10^{-1}	3.10×10^{-2}	4.57×10^{-2}	1.43×10^{-1}	2.20×10^{-2}

Table 6: Error routine- $\beta\gamma$, forecasts from 25/03

Forecast 7 days									
	SVD			NMF			Greedy		
n	$I(L^1)$	$I(L^\infty)$	$R(L^\infty)$	$I(L^1)$	$I(L^\infty)$	$R(L^\infty)$	$I(L^1)$	$I(L^\infty)$	$R(L^\infty)$
5	7.46×10^1	3.92×10^2	7.63×10^1	2.48×10^0	5.23×10^0	3.22×10^{-1}	2.65×10^{-2}	5.65×10^{-2}	3.26×10^{-2}
7	∞	∞	∞	3.57×10^0	9.95×10^0	4.31×10^{-1}	2.35×10^{-1}	5.87×10^{-1}	7.38×10^{-2}
9	∞	∞	∞	3.50×10^1	1.53×10^2	3.74×10^0	6.15×10^{-2}	9.33×10^{-2}	2.86×10^{-2}
11	∞	∞	∞	2.05×10^0	4.82×10^0	3.36×10^{-1}	3.29×10^{-1}	8.66×10^{-1}	1.00×10^{-1}
13	∞	∞	∞	7.01×10^{-1}	1.02×10^0	7.51×10^{-2}	4.96×10^{-1}	1.28×10^0	1.22×10^{-1}
15	∞	∞	∞	1.01×10^0	2.32×10^0	1.63×10^{-1}	4.98×10^{-1}	1.34×10^0	1.19×10^{-1}
17	∞	∞	∞	1.13×10^0	1.95×10^0	1.20×10^{-1}	6.79×10^{-1}	1.86×10^0	1.58×10^{-1}

Forecast 14 days									
	SVD			NMF			Greedy		
n	$I(L^1)$	$I(L^\infty)$	$R(L^\infty)$	$I(L^1)$	$I(L^\infty)$	$R(L^\infty)$	$I(L^1)$	$I(L^\infty)$	$R(L^\infty)$
5	∞	∞	∞	8.79×10^1	4.70×10^2	1.65×10^1	2.13×10^{-1}	5.27×10^{-1}	2.65×10^{-1}
7	∞	∞	∞	1.52×10^3	5.46×10^3	4.68×10^2	1.16×10^1	6.56×10^1	4.71×10^0
9	∞	∞	∞	1.75×10^3	4.84×10^3	7.69×10^2	1.87×10^0	8.62×10^0	1.17×10^0
11	∞	∞	∞	1.85×10^2	1.04×10^3	4.63×10^1	3.73×10^1	2.36×10^2	1.44×10^1
13	∞	∞	∞	2.31×10^0	5.32×10^0	5.94×10^{-1}	1.03×10^2	7.00×10^2	3.08×10^1
15	∞	∞	∞	2.10×10^2	1.46×10^3	4.44×10^1	2.26×10^2	1.63×10^3	6.42×10^1
17	∞	∞	∞	8.90×10^0	2.94×10^1	1.95×10^0	4.83×10^2	3.25×10^3	1.55×10^2

Table 7: Error routine- $\beta\gamma$, forecasts from 05/04

Forecast 7 days									
	SVD			NMF			Greedy		
n	$I(L^1)$	$I(L^\infty)$	$R(L^\infty)$	$I(L^1)$	$I(L^\infty)$	$R(L^\infty)$	$I(L^1)$	$I(L^\infty)$	$R(L^\infty)$
5	3.04×10^1	1.18×10^2	2.63×10^1	7.65×10^3	4.27×10^4	1.73×10^2	1.43×10^{-1}	1.52×10^{-1}	2.96×10^{-2}
7	9.45×10^4	$5.38e \times 10^5$	3.92×10^4	3.74×10^{-1}	5.24×10^{-1}	4.04×10^{-2}	1.01×10^{-1}	1.07×10^{-1}	2.79×10^{-2}
9	∞	∞	∞	2.46×10^{-1}	5.17×10^{-1}	2.02×10^{-2}	2.90×10^{-1}	3.40×10^{-1}	3.95×10^{-2}
11	∞	∞	∞	2.64×10^{-1}	2.62×10^{-1}	2.89×10^{-2}	6.52×10^{-2}	7.38×10^{-2}	2.10×10^{-2}
13	∞	∞	∞	2.00×10^{-1}	3.34×10^{-1}	1.73×10^{-2}	1.73×10^{-1}	2.05×10^{-1}	2.63×10^{-2}
15	∞	∞	∞	1.51×10^{-1}	3.06×10^{-1}	2.19×10^{-2}	1.64×10^{-1}	2.13×10^{-1}	2.61×10^{-2}
17	∞	∞	∞	3.63×10^{-1}	5.98×10^{-1}	3.64×10^{-2}	6.80×10^{-2}	7.99×10^{-2}	2.28×10^{-2}

Forecast 14 days									
	SVD			NMF			Greedy		
n	$I(L^1)$	$I(L^\infty)$	$R(L^\infty)$	$I(L^1)$	$I(L^\infty)$	$R(L^\infty)$	$I(L^1)$	$I(L^\infty)$	$R(L^\infty)$
5	∞	∞	∞	∞	∞	∞	2.87×10^{-1}	3.05×10^{-1}	9.02×10^{-2}
7	∞	∞	∞	8.40×10^{-1}	1.11×10^0	1.62×10^{-1}	2.33×10^{-1}	2.76×10^{-1}	8.09×10^{-2}
9	∞	∞	∞	4.05×10^0	1.79×10^1	5.46×10^{-1}	4.97×10^{-1}	4.65×10^{-1}	1.33×10^{-1}
11	∞	∞	∞	2.47×10^{-1}	2.62×10^{-1}	2.65×10^{-2}	1.85×10^{-1}	2.62×10^{-1}	5.24×10^{-2}
13	∞	∞	∞	5.56×10^{-1}	8.01×10^{-1}	9.25×10^{-2}	3.61×10^{-1}	3.79×10^{-1}	9.17×10^{-2}
15	∞	∞	∞	6.44×10^{-1}	1.35×10^0	1.26×10^{-1}	3.72×10^{-1}	4.06×10^{-1}	1.01×10^{-1}
17	∞	∞	∞	1.29×10^0	2.44×10^0	2.40×10^{-1}	1.65×10^{-1}	2.20×10^{-1}	5.60×10^{-2}

Table 8: Error routine- $\beta\gamma$, forecasts from 15/04

Observations for method routine- $\beta\gamma$:

- Using the SVD reduced bases, the 7 days and 14 days forecasts lead to large errors and even infinite errors for most cases.
- The NMF reduced basis lead to unreliable errors, for some cases it performs better than the Greedy basis but in other cases it is worse. Particularly, the error blow up when we consider the forecasts from the 05/04.
- The Greedy bases produce more accurate and consistent forecasts than SVD and NMF, we point out that the forecasts from the 05/04 are much less accurate for every method.

When the routine- $\beta\gamma$ is used, the quality of the forecast depends on the reduced basis but also strongly on the day from which the extrapolation is done. In our case the 25/03 seem to be the

case when we are able to produce the best forecasts, when the forecasts are done from 05/04 every method struggles at producing an accurate forecast. Overall for this approach the Greedy approach seem to give the best forecasts.

4.3.2 Forecasting with routine-IR

Table 9 shows the relative errors of a 7 days and 14 days forecast from 25/03 for each extrapolation method and each reduced basis. Similarly tables 10 and 11 show forecasts relative errors respectively from 05/04 and 15/04.

Forecast 7 days									
	SVD			NMF			Greedy		
n	$I(L^1)$	$I(L^\infty)$	$R(L^\infty)$	$I(L^1)$	$I(L^\infty)$	$R(L^\infty)$	$I(L^1)$	$I(L^\infty)$	$R(L^\infty)$
5	1.19×10^{-1}	1.71×10^{-1}	7.25×10^{-1}	1.14×10^{-1}	1.85×10^{-1}	2.37×10^{-1}	1.25×10^{-1}	2.03×10^{-1}	6.77×10^{-2}
7	1.19×10^{-1}	1.71×10^{-1}	7.25×10^{-1}	2.79×10^{-2}	5.19×10^{-2}	1.58×10^{-1}	1.01×10^{-1}	1.49×10^{-1}	1.02×10^{-1}
9	1.22×10^{-1}	1.74×10^{-1}	7.25×10^{-1}	2.75×10^{-1}	4.50×10^{-1}	1.87×10^{-1}	6.46×10^{-2}	1.02×10^{-1}	8.16×10^{-2}
11	1.21×10^{-1}	1.73×10^{-1}	7.25×10^{-1}	1.71×10^{-1}	2.49×10^{-1}	1.68×10^{-1}	6.48×10^{-2}	9.91×10^{-2}	7.43×10^{-2}
13	1.19×10^{-1}	1.71×10^{-1}	7.25×10^{-1}	5.59×10^{-2}	8.07×10^{-2}	5.00×10^{-2}	7.36×10^{-2}	1.30×10^{-1}	5.38×10^{-2}
15	1.19×10^{-1}	1.71×10^{-1}	7.25×10^{-1}	1.03×10^{-1}	1.42×10^{-1}	1.80×10^{-1}	4.21×10^{-2}	1.18×10^{-1}	8.48×10^{-2}
17	1.19×10^{-1}	1.71×10^{-1}	7.25×10^{-1}	2.55×10^{-2}	4.99×10^{-2}	9.98×10^{-2}	4.56×10^{-2}	1.29×10^{-1}	7.52×10^{-2}
Forecast 14 days									
	SVD			NMF			Greedy		
n	$I(L^1)$	$I(L^\infty)$	$R(L^\infty)$	$I(L^1)$	$I(L^\infty)$	$R(L^\infty)$	$I(L^1)$	$I(L^\infty)$	$R(L^\infty)$
5	1.79×10^{-1}	3.24×10^{-1}	8.41×10^{-1}	2.38×10^{-1}	3.62×10^{-1}	4.22×10^{-1}	2.66×10^{-1}	4.09×10^{-1}	2.52×10^{-1}
7	1.79×10^{-1}	3.24×10^{-1}	8.41×10^{-1}	3.91×10^{-2}	1.01×10^{-1}	2.91×10^{-1}	1.97×10^{-1}	3.04×10^{-1}	2.66×10^{-1}
9	1.77×10^{-1}	3.15×10^{-1}	8.41×10^{-1}	4.92×10^{-1}	5.78×10^{-1}	4.45×10^{-1}	1.51×10^{-1}	2.66×10^{-1}	2.50×10^{-1}
11	1.77×10^{-1}	3.17×10^{-1}	8.41×10^{-1}	2.87×10^{-1}	3.58×10^{-1}	3.59×10^{-1}	1.43×10^{-1}	2.48×10^{-1}	2.40×10^{-1}
13	1.79×10^{-1}	3.24×10^{-1}	8.41×10^{-1}	6.38×10^{-2}	9.68×10^{-2}	1.57×10^{-1}	1.92×10^{-1}	3.42×10^{-1}	2.39×10^{-1}
15	1.79×10^{-1}	3.24×10^{-1}	8.41×10^{-1}	1.57×10^{-1}	1.95×10^{-1}	3.35×10^{-1}	3.68×10^{-1}	1.17×10^0	9.41×10^{-2}
17	1.79×10^{-1}	3.24×10^{-1}	8.41×10^{-1}	1.15×10^{-1}	2.50×10^{-1}	1.59×10^{-1}	3.02×10^{-1}	8.18×10^{-1}	8.90×10^{-2}

Table 9: Error routine-IR, forecasts from 25/03

Forecast 7 days									
	SVD			NMF			Greedy		
n	$I(L^1)$	$I(L^\infty)$	$R(L^\infty)$	$I(L^1)$	$I(L^\infty)$	$R(L^\infty)$	$I(L^1)$	$I(L^\infty)$	$R(L^\infty)$
5	4.52×10^{-1}	5.50×10^{-1}	4.44×10^{-1}	1.80×10^{-1}	2.11×10^{-1}	2.23×10^{-1}	2.42×10^{-1}	3.20×10^{-1}	1.43×10^{-1}
7	4.52×10^{-1}	5.50×10^{-1}	4.44×10^{-1}	4.86×10^{-2}	1.14×10^{-1}	1.04×10^{-1}	7.18×10^{-2}	9.39×10^{-2}	1.56×10^{-1}
9	4.52×10^{-1}	5.50×10^{-1}	4.44×10^{-1}	2.34×10^{-1}	2.84×10^{-1}	2.00×10^{-1}	4.47×10^{-2}	6.56×10^{-2}	1.64×10^{-1}
11	4.52×10^{-1}	5.50×10^{-1}	4.44×10^{-1}	2.24×10^{-1}	2.40×10^{-1}	2.01×10^{-1}	1.75×10^{-1}	2.16×10^{-1}	2.04×10^{-1}
13	4.52×10^{-1}	5.50×10^{-1}	4.44×10^{-1}	2.10×10^{-1}	2.47×10^{-1}	2.09×10^{-1}	1.96×10^{-1}	2.41×10^{-1}	1.64×10^{-1}
15	4.52×10^{-1}	5.50×10^{-1}	4.44×10^{-1}	1.64×10^{-1}	2.06×10^{-1}	2.04×10^{-1}	5.86×10^{-2}	1.37×10^{-1}	1.74×10^{-1}
17	4.52×10^{-1}	5.50×10^{-1}	4.44×10^{-1}	1.56×10^{-1}	1.89×10^{-1}	2.11×10^{-1}	1.18×10^{-1}	2.99×10^{-1}	1.89×10^{-1}
Forecast 14 days									
	SVD			NMF			Greedy		
n	$I(L^1)$	$I(L^\infty)$	$R(L^\infty)$	$I(L^1)$	$I(L^\infty)$	$R(L^\infty)$	$I(L^1)$	$I(L^\infty)$	$R(L^\infty)$
5	8.05×10^{-1}	8.42×10^{-1}	5.71×10^{-1}	2.77×10^{-1}	2.56×10^{-1}	3.42×10^{-1}	4.24×10^{-1}	4.16×10^{-1}	2.84×10^{-1}
7	8.05×10^{-1}	8.42×10^{-1}	5.71×10^{-1}	3.90×10^{-1}	9.52×10^{-1}	8.32×10^{-2}	1.21×10^{-1}	1.31×10^{-1}	2.54×10^{-1}
9	8.05×10^{-1}	8.42×10^{-1}	5.71×10^{-1}	3.74×10^{-1}	3.46×10^{-1}	3.35×10^{-1}	1.55×10^{-1}	4.64×10^{-1}	2.20×10^{-1}
11	8.05×10^{-1}	8.42×10^{-1}	5.71×10^{-1}	3.09×10^{-1}	2.58×10^{-1}	3.21×10^{-1}	2.94×10^{-1}	2.90×10^{-1}	3.25×10^{-1}
13	8.05×10^{-1}	8.42×10^{-1}	5.71×10^{-1}	3.22×10^{-1}	2.91×10^{-1}	3.36×10^{-1}	2.84×10^{-1}	2.47×10^{-1}	2.82×10^{-1}
15	8.05×10^{-1}	8.42×10^{-1}	5.71×10^{-1}	2.80×10^{-1}	2.80×10^{-1}	3.26×10^{-1}	8.81×10^{-1}	3.10×10^0	1.45×10^{-1}
17	8.05×10^{-1}	8.42×10^{-1}	5.71×10^{-1}	2.45×10^{-1}	2.30×10^{-1}	3.30×10^{-1}	1.75×10^0	6.46×10^0	1.53×10^{-1}

Table 10: Error routine-IR, forecasts from 05/04

Forecast 7 days									
n	SVD			NMF			Greedy		
	$I(L^1)$	$I(L^\infty)$	$R(L^\infty)$	$I(L^1)$	$I(L^\infty)$	$R(L^\infty)$	$I(L^1)$	$I(L^\infty)$	$R(L^\infty)$
5	4.94×10^{-1}	6.10×10^{-1}	2.41×10^{-1}	2.21×10^0	4.72×10^0	7.78×10^{-2}	3.24×10^{-1}	4.78×10^{-1}	2.68×10^{-2}
7	4.94×10^{-1}	6.09×10^{-1}	2.41×10^{-1}	3.72×10^{-1}	5.86×10^{-1}	8.27×10^{-2}	2.66×10^{-1}	2.75×10^{-1}	1.18×10^{-1}
9	4.94×10^{-1}	6.09×10^{-1}	2.41×10^{-1}	1.04×10^{-1}	1.11×10^{-1}	7.99×10^{-2}	7.40×10^{-1}	1.48×10^0	8.46×10^{-2}
11	4.94×10^{-1}	6.09×10^{-1}	2.41×10^{-1}	2.19×10^{-1}	2.31×10^{-1}	1.07×10^{-1}	6.29×10^{-2}	1.05×10^{-1}	5.89×10^{-2}
13	4.94×10^{-1}	6.09×10^{-1}	2.41×10^{-1}	1.88×10^{-1}	2.61×10^{-1}	8.51×10^{-2}	8.85×10^{-1}	1.91×10^0	7.58×10^{-2}
15	4.94×10^{-1}	6.09×10^{-1}	2.41×10^{-1}	2.77×10^{-2}	4.15×10^{-2}	1.11×10^{-1}	1.22×10^{-1}	1.45×10^{-1}	1.06×10^{-1}
17	4.94×10^{-1}	6.09×10^{-1}	2.41×10^{-1}	2.59×10^{-2}	3.84×10^{-2}	1.14×10^{-1}	3.58×10^0	9.35×10^0	8.17×10^{-2}

Forecast 14 days									
n	SVD			NMF			Greedy		
	$I(L^1)$	$I(L^\infty)$	$R(L^\infty)$	$I(L^1)$	$I(L^\infty)$	$R(L^\infty)$	$I(L^1)$	$I(L^\infty)$	$R(L^\infty)$
5	8.50×10^{-1}	8.19×10^{-1}	3.37×10^{-1}	8.34×10^1	4.08×10^2	5.75×10^0	6.41×10^{-1}	6.39×10^{-1}	1.32×10^{-1}
7	8.49×10^{-1}	8.18×10^{-1}	3.37×10^{-1}	1.04×10^0	1.60×10^0	9.06×10^{-2}	4.33×10^{-1}	3.96×10^{-1}	2.09×10^{-1}
9	8.49×10^{-1}	8.18×10^{-1}	3.37×10^{-1}	2.06×10^{-1}	2.40×10^{-1}	1.44×10^{-1}	2.37×10^1	1.24×10^2	1.44×10^0
11	8.50×10^{-1}	8.18×10^{-1}	3.37×10^{-1}	3.93×10^{-1}	3.81×10^{-1}	1.93×10^{-1}	6.48×10^{-2}	1.05×10^{-1}	9.70×10^{-2}
13	8.50×10^{-1}	8.18×10^{-1}	3.37×10^{-1}	2.91×10^{-1}	2.61×10^{-1}	1.35×10^{-1}	7.44×10^1	4.56×10^2	4.44×10^0
15	8.49×10^{-1}	8.18×10^{-1}	3.37×10^{-1}	1.02×10^{-1}	1.76×10^{-1}	1.81×10^{-1}	2.86×10^{-1}	3.29×10^{-1}	1.89×10^{-1}
17	8.49×10^{-1}	8.18×10^{-1}	3.37×10^{-1}	2.52×10^{-2}	3.84×10^{-2}	1.78×10^{-1}	2.26×10^3	1.17×10^4	1.60×10^2

Table 11: Error routine-IR, forecasts from 15/04

Observations for the method routine- $\beta\gamma$:

- Using the SVD reduced bases, the 7 days and 14 days forecasts lead to large errors and even infinite errors for most cases.
- The NMF reduced basis lead to unreliable errors, for some cases it performs better than the Greedy basis but in other cases it is worse and sometimes the error blow up particularly when we consider the forecasts from the 05/04.
- The Greedy bases produce more accurate and consistent forecasts than SVD and NMF, we point out that the forecasts from the 05/04 are much less accurate for every method and even the Greedy basis struggles not to blow up the error.

When the routine- $\beta\gamma$ is used, the quality of the forecast depends on the reduced basis but also strongly on the day from which the extrapolation is done. In our case the 25/03 seem to be the case when we are able to produce the best forecasts and when the forecasts are done from 05/04 every method struggles at producing an accurate forecast. Overall for this approach the greedy approach seem to give the best forecasts.

Observations for the method routine-IR:

- In this case the forecasts obtained by SVD reduced bases are not accurate as the optimisation method to obtain them did not converge in every case.
- The accuracies obtained by NMF and Greedy are very similar with slightly more reliability for NMF as the error never blows up whereas the greedy forecasts blow up in some cases when the forecast is done from the 15/04.

routine-IR shows much more stability than routine- $\beta\gamma$ as the forecast error is less sensitive on the arbitrary number of modes used for the reduced basis. Overall NMF seem to be the most reliable option to perform a forecast for routine-IR.

4.4 Examples of prediction

In this section we show the result of the extrapolation for both methods.

- For routine- $\beta\gamma$ a Greedy reduced basis is used with dimension $n = 9$.
- For routine-IR a NMF reduced basis is used with dimension $n = 15$.

Figures 5, 6 and 7 show respectively the forecasts from the 25/03, 05/04 and 15/04 for the number of infected and for the number or recovered.

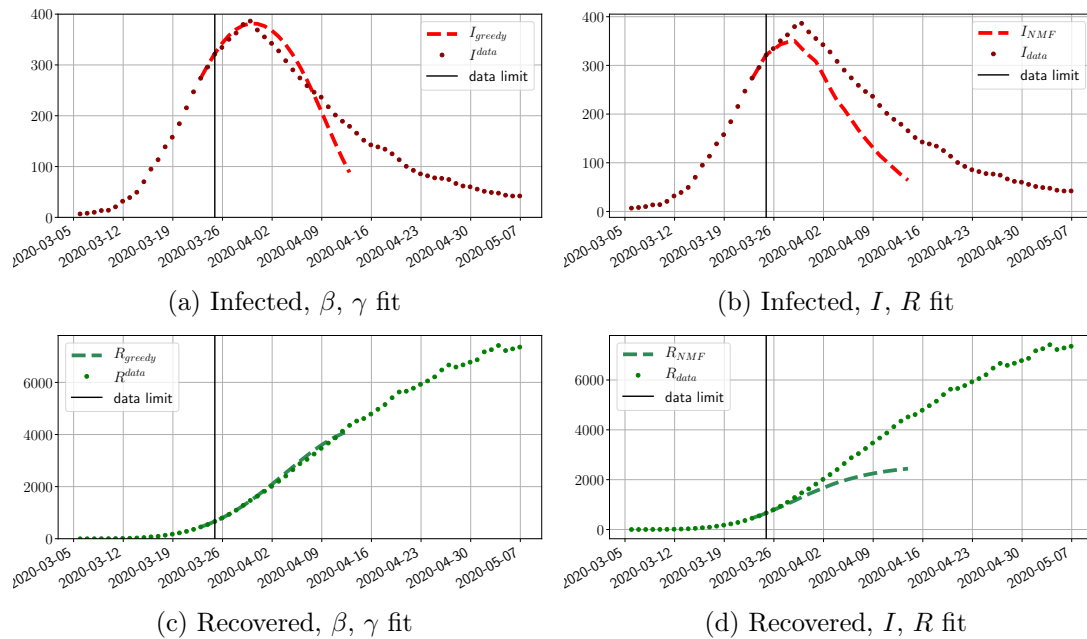


Figure 5: Forecasts from 25/03

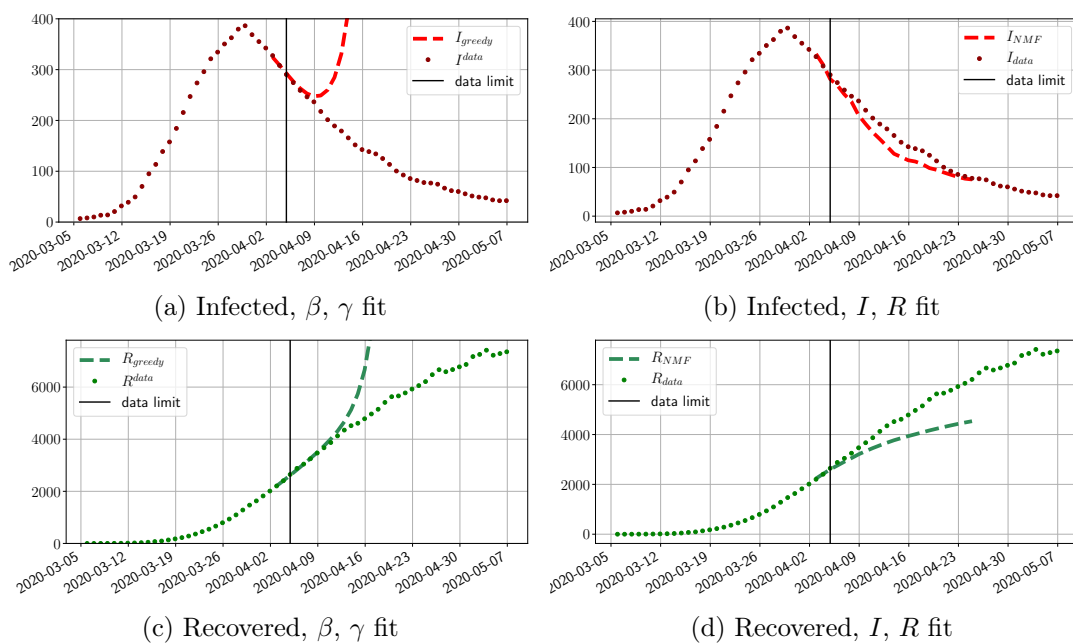


Figure 6: Forecasts from 05/04

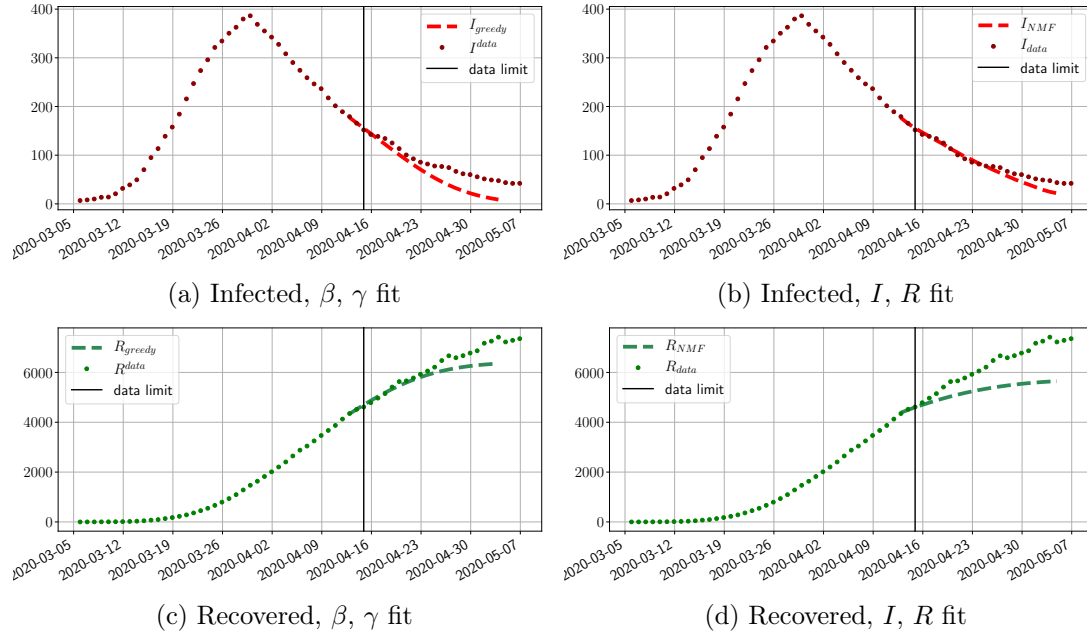


Figure 7: Forecast from 15/04

The comparisons done here between the two forecasting methods show that, in our examples, **routine-IR** seems to be more robust as it does not bow up when **routine- $\beta\gamma$** does, as we can see in Figure 6. Figure 5 shows a better approximation using **routine- $\beta\gamma$** for the number of infected and recovered. Figure 7 shows similar results for the extrapolation of the number of recovered but a much more accurate extrapolation for the number of infected with **routine-IR**.

5 Acknowledgments

We would like to thank our colleagues from the “Face au virus” initiative in PSL University: Jamal Atif, Laurent Massoulié, Olivier Cappé, and Akin Kazakcy. We also thank Gabriel Turinici for his feedback on the multiregional models. Finally, we are grateful to the DREES for providing the health data. Part of this research has been supported by the Emergences project grant “Models and Measures” of the Paris city council, by the generous donation made available by Alkan together with the complementary funding given by the Sorbonne University Foundation. This research is done in the frame of the project Pandemia/Covidia and also the GIS Obepine, both projects aiming at a better understanding of the Covid-19 pandemic.

References

- [1] Atif, J., Cappé, O., Kazakçı, A., Léo, Y., Massoulié, L. and Mula, O. Initiative face au virus Observations sur la mobilité pendant l’épidémie de Covid-19. Technical report, Université PSL, May 2020. URL <https://hal.archives-ouvertes.fr/hal-02921194>.
- [2] Di Domenico, L., Pullano, G., Sabbatini, C. E., Boëlle, P.-Y. and Colizza, V. Impact attendu du confinement en Ile-de-France et stratégie de sortie possibles. URL www.epicx-lab.com/covid-19.html.
- [3] Gillis, N. The why and how of nonnegative matrix factorization. *Regularization, optimization, kernels, and support vector machines*, 12(257), pp. 257–291, 2014.

- [4] Kermack, W. O., McKendrick, A. G. and Walker, G. T. A contribution to the mathematical theory of epidemics. *Proceedings of the Royal Society of London. Series A, Containing Papers of a Mathematical and Physical Character*, 115(772), pp. 700–721, 1927. URL <http://dx.doi.org/10.1098/rspa.1927.0118>.
- [5] Magal, P. and Webb, G. Predicting the number of reported and unreported cases for the COVID-19 epidemic in South Korea, Italy, France and Germany. *medrxiv*, 2020. URL <https://doi.org/10.1101/2020.03.21.20040154>.
- [6] Paatero, P. and Tapper, U. Positive matrix factorization: A non-negative factor model with optimal utilization of error estimates of data values. *Environmetrics*, 5(2), pp. 111–126, 1994. URL <https://doi.org/10.1002/env.3170050203>.
- [7] Poncela, P., Rodríguez, J., Sánchez-Mangas, R. and Senra, E. Forecast combination through dimension reduction techniques. *International Journal of Forecasting*, 27(2), pp. 224–237, April 2011. URL <https://ideas.repec.org/a/eee/intfor/v27yi2p224-237.html>.